Fortschr. Phys. **54**, No. 8 – 10, 776 – 787 (2006) / **DOI** 10.1002/prop.200610318

Prospects of ultracold Rydberg gases for quantum information processing

Markus Reetz-Lamour[1]*, **Thomas Amthor**[1], **Johannes Deiglmayr**[1], **Sebastian Westermann**[1], **Kilian Singer**[1] **, **André Luiz de Oliveira**[2] ***, **Luis Gustavo Marcassa**[2], and **Matthias Weidemüller**[1] #

[1] Physikalisches Institut der Universität Freiburg, Hermann-Herder-Str. 3, 79104 Freiburg, Germany
[2] Instituto de Física, Universidade de São Paulo, São Carlos, SP 13560-970, Brazil

Published online 4 August 2006

Key words Ultracold, Rydberg, quantum, information
PACS 32.80.Rm, 03.67.Lx, 32.80.Pj, 34.20.Cf

We present our experiments on the applicability of ultracold Rydberg gases for quantum information processing. As quantum computing relies on entanglement mediated through interparticle interactions, we have experimentally implemented three approaches to induce ultralong-range interactions between Rydberg atoms: van-der-Waals interactions, interactions of permanent dipoles induced by an electric field, and resonant dipole-dipole interactions (Förster resonances). Advantages and limitations of the approaches are discussed.

© 2006 WILEY-VCH Verlag GmbH & Co. KGaA, Weinheim

1 Introduction

During the past ten years, we have witnessed a tremendous progress towards the physical realization of quantum computers. Among the most promising concepts are trapped ions, atoms interacting with photons in high-Q cavities, and nuclear spins in combination with NMR methods [1, 2]. The essential feature of these systems is the ability to create entanglement via controlled interactions. Besides these systems, neutral atoms are particularly attractive candidates for quantum information processing because of their relatively weak coupling to dissipative processes of the environment, the ability to precisely manipulate internal and motional degrees of freedom and the possibility to achieve long coherence times [3, 4]. Therefore, several schemes were proposed to entangle neutral atoms for the realization of quantum gates with considerable fidelity [5]. However, entanglement between neutral atoms is hard to achieve due to the weakness of their mutual interactions, in contrast to, *e.g.*, the long-range Coulomb force acting between charged particles. Proposed mechanisms for obtaining entanglement between neutral atoms leading to the realization of quantum gates employ cold collisions [6], optically controlled ground-state interactions [7] and dipole-dipole interactions [8, 9].

Rydberg atoms appear to be particularly well suited for quantum information processing [8, 9]. They exhibit extremely long-range dipolar forces due to the strong polarizability of the weakly bound outer electron, which scales as n^7 (n denotes the principal quantum number of the atom). The relevant qubits are either two ground states of a single atom [8], or collective states of the multi-particle ensemble [9].

* E-mail: m.rlamour@physik.uni-freiburg.de
** Present address: Abteilung Quanten-Informationsverarbeitung, Universität Ulm, Albert-Einstein-Allee 11, 89069 Ulm, Germany.
*** Permanent address: Departamento de Física, Universidade do Estado de Santa Catarina, Joinville, SC 89223-100, Brazil.
# Corresponding author E-mail: m.weidemueller@physik.uni-freiburg.de

© 2006 WILEY-VCH Verlag GmbH & Co. KGaA, Weinheim

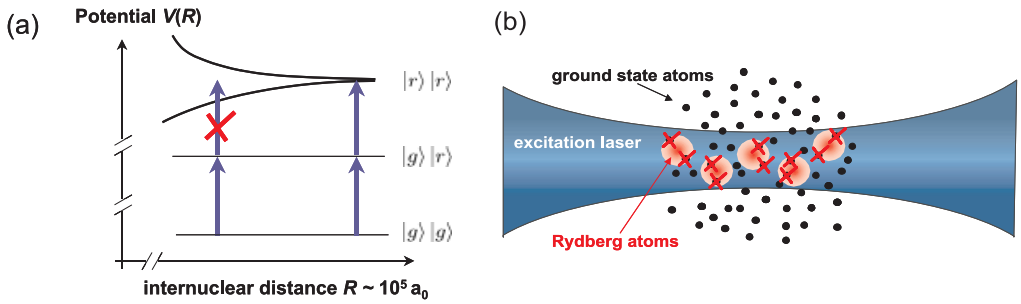

Fig. 1 Explanation of the dipole blockade. (a) Simplified presentation of the dipole blockade with only one pair of atoms being involved. $|g\rangle$ and $|r\rangle$ denote the ground and Rydberg state, respectively. The ultralong range dipole interaction splits the Rydberg pair state and thus suppresses excitation of a Rydberg pair by a resonant laser field, as indicated by the vertical arrows. (b) Local dipole blockade. An excitation laser beam is overlapped with a cloud of cold atoms. Rydberg excitation out of the gas is suppressed in the vicinity of a Rydberg atom by the interaction, resulting in the local dipole blockade.

The many-body approach also solves the ubiquitous problem of addressability. Instead of addressing single atoms, which requires very high optical resolution and detection efficiency, single Rydberg excitation in a mesoscopic ensemble is enforced by the so-called "dipole blockade", i.e. the suppression of many-body states with more than a single excitation through the strong dipole-dipole interaction between Rydberg atoms. Employing the dipole blockade, several mesoscopic systems may be used to perform gate operations, by either transferring qubits between distant systems or by direct dipole-dipole interaction of two closely spaced systems.

A simplified picture of the blockade effect is shown in Fig. 1. At large internuclear separations, Rydberg atoms are resonantly excited by a laser field indicated by the arrows in Fig. 1(a). When the internuclear distance is decreased, the dipole interaction between pairs of Rydberg atoms splits the energy levels, thus shifting the Rydberg pair out of resonance with the laser and impeding the excitation of a Rydberg pair. As indicated in Fig. 1(b), each Rydberg atom in a gas defines a volume in which no further Rydberg states can be excited. The size of the volume is given by the condition that the interaction energy is larger than the linewidth of the single-Rydberg excitation line. As a consequence, further Rydberg excitation is locally blocked around each Rydberg atom resulting in optically addressable domains with a well defined excitation (local dipole blockade).

To realize fast phase gates for quantum computation involving Rydberg atoms, the atoms are either entangled by the interaction of the permanent dipole moments of Rydberg states in a static electric field, or by the dipole interaction (van-der-Waals interactions or Förster resonant energy exchange). The Förster process has recently been experimentally demonstrated in a frozen Rydberg gas [10,11]. In order to use this process for gate operations, the atomic center-of-mass has to be stationary in order to avoid entanglement between internal and motional degrees of freedom. Therefore, ultracold samples of atoms have to be used. To realize quantum logic operations with Rydberg atoms, it is mandatory to enter a regime in which the dipole-dipole interaction governs the internal dynamics of the system. However, it has been shown that cold Rydberg gases at high densities tend to spontaneously evolve into ultracold plasmas [12] or may undergo strong ℓ-mixing processes thus forming high-angular-momentum states [13]. Both effects destroy the entanglement since the interaction between the Rydberg atoms is strongly modified. In particular, free charges igniting the evolution into a plasma have to be excluded.

In this article we describe our experiments towards the implementation of quantum information processing with Rydberg atoms. We have explored the prospects of three different scenarios for the creation of strong interparticle forces as a prerequisite for fast quantum gates: van-der-Waals interactions, interactions

© 2006 WILEY-VCH Verlag GmbH & Co. KGaA, Weinheim

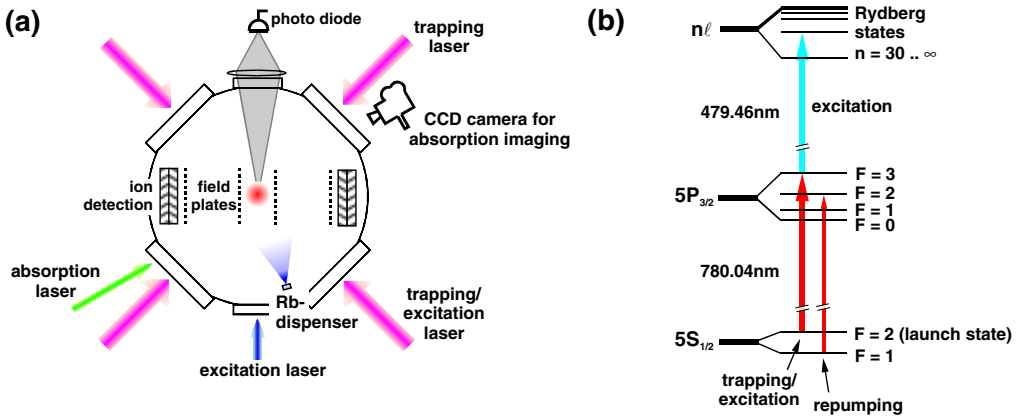

Fig. 2 (a) Experimental setup for the preparation of a frozen Rydberg gas from a magneto-optical trap. (b) Relevant energy levels for the two-photon excitation of ^{87}Rb Rydberg atoms. The population of the launch state $5S_{1/2}(F=2)$ can be controlled by depumping atoms to the dark $5S_{1/2}(F=1)$ state.

of permanent dipoles, and Förster resonances (resonant dipole-dipole interactions). Signatures of these interactions are discussed in sections 3, 4, and 5, respectively. Sect. 2 gives an overview over the experimental setup. A short summary and outlook is given in section 6.

2 Excitation of Rydberg atoms from an ultracold gas

The experimental setup is described in detail in [14]. Grating stabilized diode lasers are used to trap a cloud of cold ^{87}Rb atoms in a magneto-optical trap (MOT) as schematically shown at the center of Fig. 2(a). The MOT is placed between two metal grids (1.5cm apart) with high optical transmission which are used to apply electric fields during excitation and to field-ionize the Rydberg atoms. The resulting ions and electrons are accelerated by electric fields and detected by micro-channel plates (MCP). Between 10^7 and 10^8 ^{87}Rb atoms are typically trapped at a peak density of about $10^{10}\mathrm{cm}^{-3}$ with loading times of roughly 5 s. The steady state temperature of the MOT is about 200 µK. The temperature can be reduced in pulsed operation down to 4.5 µK using optical molasses or below 1 µK with 3D degenerate Raman sideband cooling [15,16].

The cold atoms are prepared in Rydberg states by a a two-photon excitation scheme shown in Fig. 2(b). The first photon is provided by a commercial high-power diode laser with a line width $\lesssim 1$ MHz (Toptica, DLX 110), while the second photon is generated by a commercial cw laser system consisting of a frequency-doubled semiconductor laser source with a line width <2 MHz (Toptica, TA-SHG 110). The wavelength of this laser can be tuned to address Rydberg levels starting from $n \simeq 30$ up to the ionization threshold. All lasers can be independently switched by accousto-optical modulators with switching times in the 100-ns range.

In a typical experimental cycle (repeated every 70 ms) the MOT lasers are switched off 3ms after the quadrupole magnetic field used for trapping is turned off. The red and blue excitation lasers are switched on for a variable time period. The cycle is completed by ionizing the Rydberg atoms with either an electric field pulse or ramp and detecting the resulting ions and electrons on two opposite MCPs. The MCP signals are calibrated by comparison with the loss in MOT fluorescence. The density of Rydberg atoms can be controlled by varying the population in the $5S_{1/2}(F=2)$ launch state through optical pumping into the $5S_{1/2}(F=1)$ state.

A recent improvement to the experiment is an active frequency stabilization for the blue excitation laser. While all other lasers are stabilized via Doppler-free Rb spectroscopy, no such reference is available for the

© 2006 WILEY-VCH Verlag GmbH & Co. KGaA, Weinheim

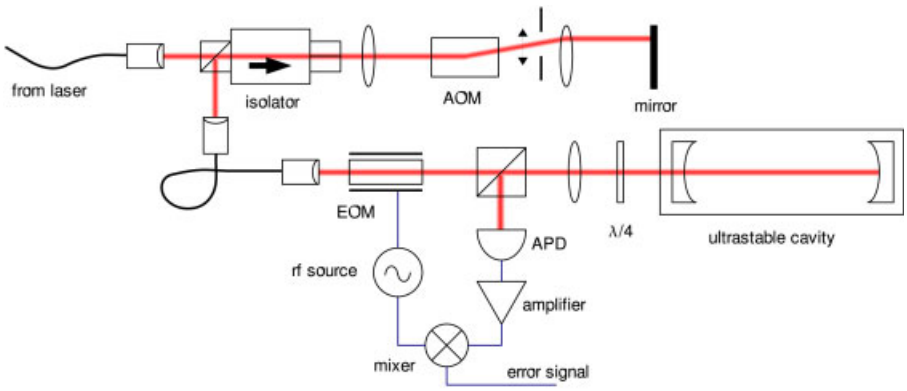

Fig. 3 Simplified sketch of the frequency stabilization of the Rydberg excitation laser at 480 nm. The laser passes through an optical isolator and an accousto-optical modulator (AOM) in double-pass configuration. The frequency-shifted reflected beam is guided through another fiber, modulated by an electro-optical modulator (EOM) and coupled into the ultrastable cavity. An avalanche photo diode (APD) picks up the reflected beam. The output is amplified and mixed with the modulating signal to obtain an error signal for locking the laser.

blue laser which has to be stabilized over a wide range of optical frequencies. We use an ultrastable cavity made of ZERODUR® as a reference. A monitor beam of the fundamental laser is tuned by a wide-range accousto-optical frequency shifter onto a cavity mode and stabilized by frequency modulation techniques (see Fig. 3). The optical power at the photodiode is as low as 100 nW while the amplification stage of the photodiode still provides a bandwidth of 10 MHz. With this scheme, the excitation laser at 480 nm can be stabilized with an absolute frequency stability better than 1 MHz over a period of one hour.

3 Van-der-Waals interaction

Van-der-Waals (vdW) interaction is the weakest interaction between neutral atoms and typically depends on the interatomic distance R as C_6/R^6. However, due to the high polarizability of Rydberg atoms the interaction strength increases drastically ($C_6 \propto \mathsf{n}^{11}$) with the principal quantum number n [17,18]. Van-der-Waals interaction therefore provides strong interaction for high-n states and seems promising for demonstrating an excitation blockade.

3.1 Blockade of excitation

Clear evidence of a local blockade due to van-der-Waals interaction has recently been reported by a group at the University of Connecticut [19] and by our group [20]. In the Connecticut experiment, Rydberg atoms are excited by a single-photon, pulsed laser excitation. Saturation of Rydberg excitation was observed with increasing laser power for highly-excited Rydberg states ($\mathsf{n} \simeq 70$) while no saturation was present for states with low quantum numbers ($\mathsf{n} \simeq 30$). Care was taken to exclude that the saturation was induced by power saturation or saturation of the MCP detectors. The observed suppression of Rydberg excitation could quantitatively be described by a theoretical mean-field model which is based on a solution of the optical Bloch equations for an atom interacting with nearby Rydberg atoms. Besides a suppression of Rydberg excitation with increasing laser intensity, the dipole blockade was also observed by increasing the density of launch state atoms.

Equivalent to this approach for the investigation of the dipole blockade, we have recorded excitation spectra of the $82S_{1/2}$ state at different Rydberg densities [20]. The density is changed by either varying

 © 2006 WILEY-VCH Verlag GmbH & Co. KGaA, Weinheim

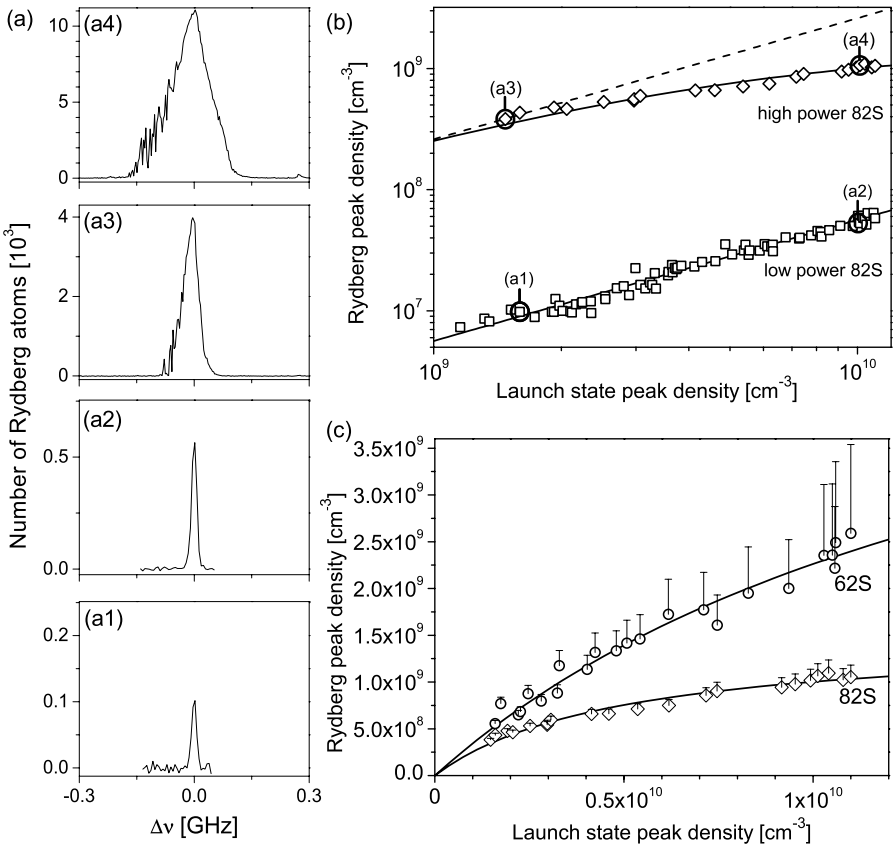

Fig. 4 (a) Excitation spectra of the $82S_{1/2}$ state at different intensities of the blue excitation laser [6 W/cm^2 for (a1) and (a2), 500 W/cm^2 for (a3) and (a4)] and launch state densities [(a1) 1.6×10^9 cm^{-3}, (a2) 1.0×10^{10} cm^{-3}, (a3) 1.5×10^9 cm^{-3}, (a4) 1.0×10^{10} cm^{-3}]. (b) Rydberg peak densities on the $82S_{1/2}$ resonance versus launch state density for 6 W/cm^2 (□) and 500 W/cm^2 (◇). The dashed line is a linear extrapolation from the origin through the first data point. Data points corresponding to the spectra (a1) to (a4) are marked. (c) Comparison of the density-dependent suppression of Rydberg excitation for the $82S_{1/2}$ (same data as in (b)) and $62S_{1/2}$ (◯) resonances. The $62S_{1/2}$ data were taken at 350 W/cm^2. The solid lines in (b) and (c) show fitted saturation functions. The upper error bars are caused by assuming that the maximum measured signals fully saturate the MCP. We see that the MCP saturation hardly affects the 82S data.

the power of the excitation laser or by changing the density of atoms in the $5S_{1/2}$(F=2) launch state. We observe a significant broadening of the S line with increasing density. The line broadening is accompanied by suppression of excitation on resonance as shown in Fig. 4. If no interaction is present, the peak density of Rydberg atoms $\hat{n}_{\rm Ryd}$ scales linearly with the launch state density $\hat{n}_{\rm g}$. This is indeed realized in the "low intensity" regime as a fit to the data yields $\hat{n}_{\rm Ryd} = p_{82,\rm low}\, \hat{n}_{\rm g}^{0.99(2)}$, with $p_{82,\rm low}$ being the excitation probability at low laser intensities. In the "high intensity" regime, however, the increase of Rydberg density scales less than linearly with $\hat{n}_{\rm g}$ clearly showing the onset of an excitation blockade as schematically depicted in Fig. 1. At high excitation rate and density, we detect only 10^4 Rydberg atoms, which is a factor of ~ 2.7 less than expected from simple linear density scaling indicated by the dashed line in Fig. 4. It is important to note that power saturation cannot explain the *density-dependent* saturation of the Rydberg excitation since it would still lead to a linear dependence of the Rydberg density on the launch state density.

© 2006 WILEY-VCH Verlag GmbH & Co. KGaA, Weinheim

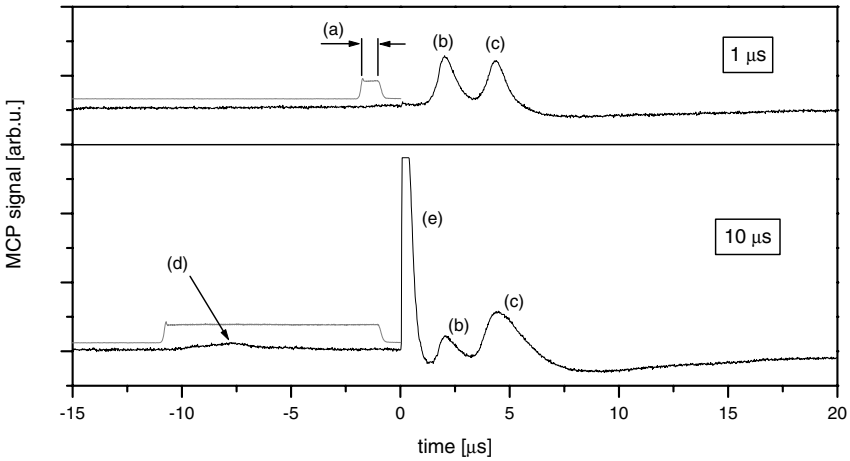

Fig. 5 Electron signals of the $82S_{1/2}$ state excited with two different excitation times of 1 µs (upper graph) and 10 µs (lower graph). The gray line depicts the time and duration of the blue excitation laser (a). At zero time a rising electric field ramp is applied. This leads to the detection of electrons obtained by field ionization of the initially excited Rydberg state (b) and (c). For excitation times of 10 µs two additional features occur: Approximately 2 µs after starting the excitation pulse free electrons from spontaneously generated ions are visible (d) and right after starting the field ramp trapped electrons from the neutral plasma are detected (e). See text.

We have also compared the saturation for different principal quantum numbers. The vdW interaction potential between two Rydberg atoms strongly increases with the principal quantum number. Therefore, one expects weaker suppression of Rydberg excitation for lines with lower principal quantum number, although the transition strength of these lines is much higher. Indeed we observed that the $82S_{1/2}$ line saturates at significantly smaller launch state densities than the $62S_{1/2}$ line. Additionally, the asymptotic Rydberg saturation density for $62S_{1/2}$ excitation relative to $82S_{1/2}$ excitation is larger by factor of 3.4.

3.2 Ionization

Interactions in cold Rydberg gases can also be induced by ions present in the sample. These ion-Rydberg atom interactions strongly perturb the Rydberg excitation spectra and impede the use of Rydberg atoms for quantum information processing. It is therefore crucial to understand how ions are formed out of a gas of Rydberg atoms (see also [21]).

To this aim we have investigated the dynamics of ion formation. After excitation with a variable duration of the laser pulse we detect Rydberg atoms with state-selective field ionization. In this way, different Rydberg states and ions can be distinguished. Fig. 5 shows the electron signal for different excitation times monitored while the field is ramped up for ionization. For short excitation pulses, only Rydberg atoms are detected (see signals (b) and (c) in Fig. 5). The two peaks in the signal represent atoms in the initially excited $82S_{1/2}$ state. As the electric field is ramped up for ionization, atoms in the 82S state are diabatically transferred to states with higher angular momentum. As these states are ionized at higher fields, the characteristic electron signal of S states is a double peak structure.

When the excitation time is increased a small electron signal is detected during laser excitation (see signal (d) in Fig. 5). The origin of the electrons is discussed in the next paragraph. As these electrons leave the cloud, the much heavier cold ion cores remain, forming an electrostatic potential well for subsequently produced electrons [12]. Electrons are trapped in the potential of these ion cores, thus forming a neutral plasma with the ions. In an avalanche process, these trapped electrons ionize more Rydberg atoms through electron impact. When the electric field is ramped up, plasma electrons are released from the Coulomb

 © 2006 WILEY-VCH Verlag GmbH & Co. KGaA, Weinheim

trough and appear at much lower fields (signal (e) in Fig. 5) than the electrons produced by the ionization of bound Rydberg states.

While the avalanche-like formation of the cold plasma by electron impact ionization is well understood, the initial ionization process producing free electrons remained obscure. Collisions with hot background atoms occur at a rate of 200 Hz while blackbody radiation leads to an ionization rate below 3 kHz [22]. Both processes can therefore not account for the initial electrons triggering the plasma formation. Recently, Li et al. [23] pointed out that the initially frozen gas can pick up kinetic energy due to the interaction of Rydberg atoms. We are currently performing further measurements on this initial ionization process [16].

In order to suppress effects of motion and/or ionization one has to work at timescales that are shorter than typical timescales for ionization. As the excitation rate scales with $1/\mathsf{n}^3$ lower n states are needed for short excitation times [22]. However, since van-der-Waals interaction ($\propto \mathsf{n}^{11}$) is smaller for lower n, stronger interactions are required, *e.g.* dipole-dipole interactions.

4 States with permanent electric dipole moments

In the previous section induced electric dipole interactions (van-der-Waals interactions) were discussed. The interaction energy of induced dipoles scales as $1/R^6$ with interatomic distance R. Permanent dipole-dipole interactions exhibit a $1/R^3$ scaling law and is therefore dominating the vdW-interaction at large interatomic distances R. It can thus be detected even at lower principal quantum number n.

Permanent dipole moments can be produced by applying an electric field to the atom sample mixing states with different orbital momentum projection. The dipole moment can be determined by the electric field dependence (i.e. the Stark shift) of the resonance lines. As the energy of an electric dipole μ in an

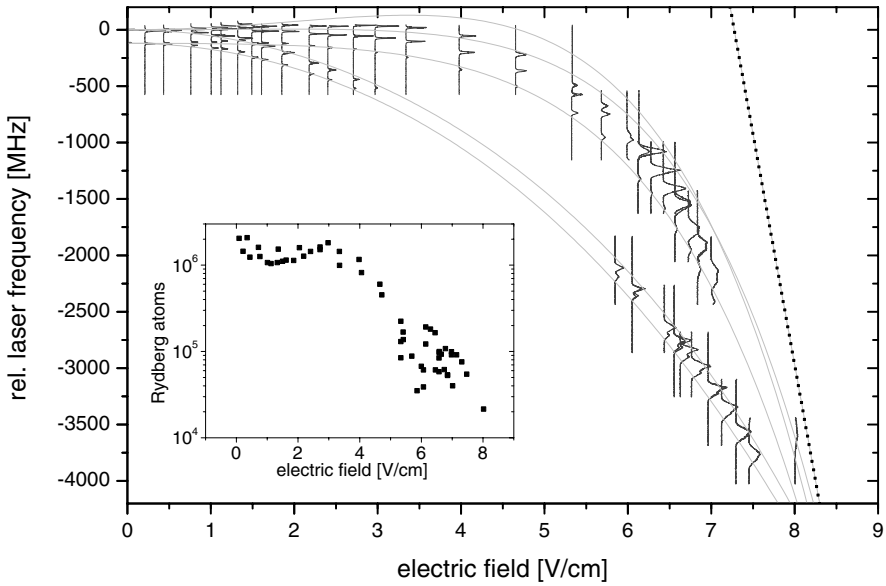

Fig. 6 Electric field dependence (Stark map) of the $46D_{5/2}$ and $46D_{3/2}$ states. The electric field lifts the degeneracy of the m_J sublevels. Resonances that shift with the electric field belong to states with a permanent dipole moment. The solid grey lines are calculated. The measured spectra are enlarged at high electric fields because of the decreasing excitation rate. The desired dipole moment of 4.1 GHz/(V/cm) (see text) is indicated as a dotted line at the right hand side. The inset shows the maximum number of Rydberg atoms detected at each electric field. At 8 V/cm the excitation rate has already decreased by two orders of magnitude.

© 2006 WILEY-VCH Verlag GmbH & Co. KGaA, Weinheim

electric field $\mathcal{E}$ scales as $\mu \cdot \mathcal{E}$ the dipole moment can be directly measured as the slope of the lines in a Stark map (see Fig. 6).

The dipole interaction energy for a pair of atoms is given by

$$V_{\rm dd} = \frac{1}{4\pi\varepsilon_0}\frac{\mu^2}{R^3} \ . \tag{1}$$

When exciting with a laser linewidth of a few MHz, an interaction energy corresponding to a frequency of $V_{\rm dd}/h \sim 10\,\text{MHz}$ is needed at the typical distance of atoms in an ultracold sample of about 10 µm in order to achieve a blockade effect. This gives a necessary dipole moment of $\mu = 3200 e a_0 = 4.1\,\text{GHz}/(\text{V}/\text{cm})$. For instance the $46\text{D}_{5/2}$ state in Rb has such a dipole moment at a very moderate electric field of 10.5 V/cm.

We have measured the corresponding Stark map which is shown in Fig. 6. The measured spectra at different electric fields are overlayed by calculated positions of the spectral lines in an electric field [24]. Note that the excitation rate drops drastically as the electric field is increased. The inset of Fig. 6 shows the maximum number of detected Rydberg atoms at different electric fields. At 8 V/cm, their number has already decreased by two orders of magnitude. So while the dipole moment is sufficient, the low excitation rate makes it difficult to excite a high enough density in order to observe a dipole blockade. There are three possible ways to overcome this problem and to make interactions between permanent dipole moments amendable for quantum information processing. One possibility consists in an increase of the density by state-of-the-art techniques for quantum gases. An alternative way consists of exciting the states at small fields and to transiently switch the field to the desired higher value. Other states with comparable dipole moments are hydrogen-like states. These, however, cannot be excited to high enough densities with our current laser setup but one can use an additional excitation step in order to obey the selection rules for dipole excitation.

5 Förster resonances

Besides using permanent dipoles one can also resonantly enhance the interaction strength using two-particle resonances. Resonant energy transfer collisions occur when one collisional partner loses as much internal energy as the other one gains. While molecules offer many close-lying levels for such resonant collisions, atoms rely on coincidentally resonant states. Rydberg states however can easily be shifted by electric fields and therefore constitute a perfect tool to study these resonant energy transfer collisions [25]. The exact electric field value needed to tune in to these so-called Förster resonances depend on the quantum defects of the atom used. Rubidium offers two possible processes, namely

$$\mathsf{n}\text{P} + \mathsf{n}\text{P} \rightleftharpoons \mathsf{n}\text{S} + (\mathsf{n}+1)\text{S} \tag{2}$$

and

$$\mathsf{n}\text{D} + \mathsf{n}\text{D} \rightleftharpoons (\mathsf{n}+2)\text{P} + (\mathsf{n}-2)\text{F} \ , \tag{3}$$

which can be tuned to resonance at reasonable electric fields due to the different Stark shifts of the involved states.

Förster resonances are of interest because a simple change in the electric field turns the interaction from off-resonant van-der-Waals ($V_{\rm dd} = (\sqrt{2}\mu\mu')^2/(\Delta\, R^6)$ in a.u.) to on-resonant dipole-dipole ($V_{\rm dd} = \sqrt{2}\mu\mu'/R^3$) interaction. Fig. 7 compares the interaction potentials of two atoms in the 46D state for these cases. The strength changes by more than one order of magnitude at the typical interatomic spacing of 5 µm underlining the great amount of control Förster resonances offer.

We have experimentally explored this resonance: We excite the atom cloud to the $46\text{D}_{5/2}$ state and then switch the electric field to a variable value $\mathcal{E}$ for 1 µs after which the atom cloud is ionized by applying a field ramp. Since 46D and 48P ionize at different electric fields they can be distinguished by their arrival

 © 2006 WILEY-VCH Verlag GmbH & Co. KGaA, Weinheim

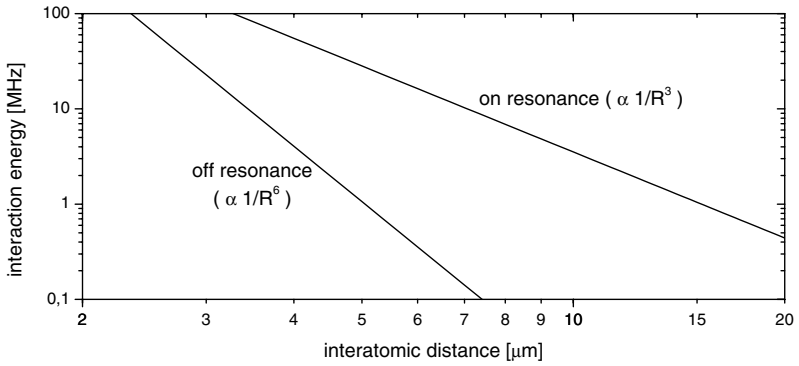

Fig. 7 Comparison of the on-resonant and off-resonant interaction for the Förster process (3) at n=46. The dipole moments $\mu = \langle 46\mathrm{D}|\, er\, |48\mathrm{P}\rangle$ and $\mu' = \langle 46\mathrm{D}|\, er\, |44\mathrm{F}\rangle$ are both $\simeq 1600$a.u. Note that the potentials are simplified not taking all possible molecular symmetries into account (see text).

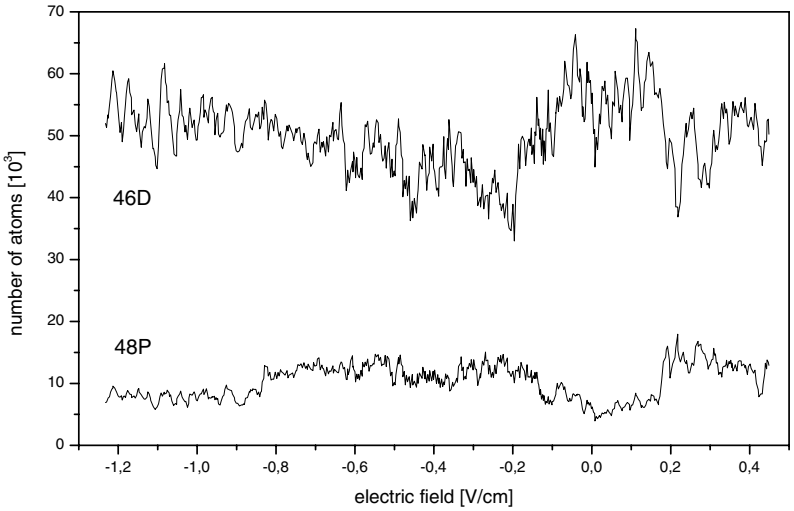

Fig. 8 When setting the excitation laser to the 46D resonance, also 48P atoms are detected due to the energy transfer process (3). The upper trace shows the 46D atoms initially excited, the lower trace shows the 48P atoms due to redistribution. The atom numbers for the different states depend on the electric field as this transfer process is resonant at a field of $\pm$ 0.25 V/cm.

time on the detector. Fig. 8 shows the number of 48P atoms depending on the chosen electric field. The resonance can be seen as an increase of 48P atoms at electric fields $|\mathcal{E}| \simeq 0.25$V/cm. It broadens to the high-field side, which we attribute to the fact that the 44F state can mix with higher angular momentum states which are energetically almost degenerate.

Walker and Saffman [26] pointed out that the simple picture of Fig. 7 is not valid. In fact molecular symmetries have to be considered, which can lead to negligible interaction strengths for some symmetries even in the on-resonant case. This shows the importance of control over the excitation process. For example, excitation to specific sublevels can reduce the number of involved molecular states. In particular our narrow-bandwidth laser system allows to distinguish different $|\mathrm{m_J}|$ levels when exciting in electric fields and can therefore show complementary results to setups with broadband pulsed lasers.

© 2006 WILEY-VCH Verlag GmbH & Co. KGaA, Weinheim

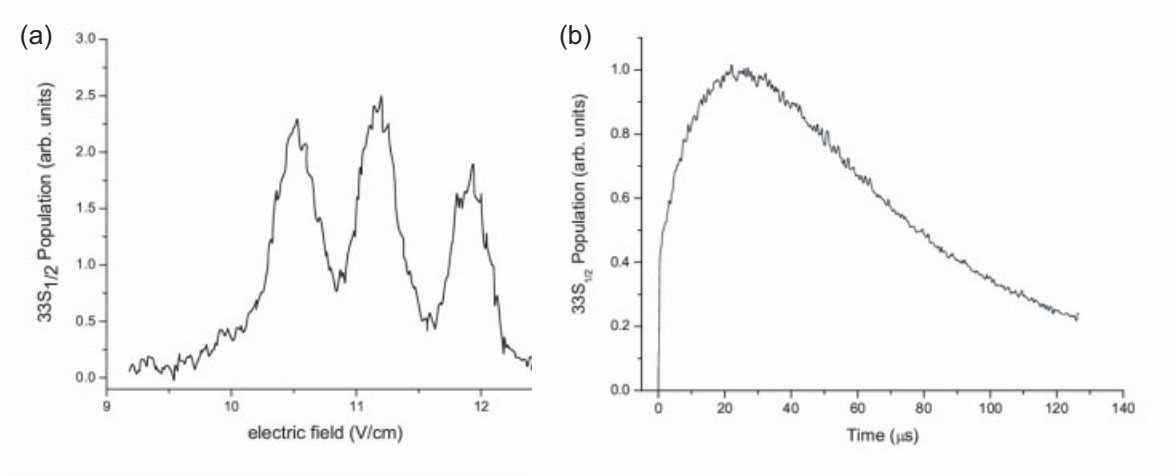

Fig. 9 (a) Population of the $33S_{1/2}$ when exciting to the $32P_{3/2}$ state and scanning the electric field over the Förster resonance. Three resonances appear which correspond to the different combinations of involved $|m_J|$ levels. In a setup with a narrowband laser, different $|m_J|$ values are spectroscopically resolved and only one resonance would appear. (b) Evolution of the $33S_{1/2}$ signal at an electric field of 10.4 V/cm. The initial increase up to 20 µs has been attributed to atomic motion while the slow decay is due to the finite lifetime of the $33S_{1/2}$ state.

As a first step, in a joined experiment carried out in São Carlos, we have therefore studied the following collisional process in rubidium:

$$32P_{3/2} + 32P_{3/2} \longrightarrow 32S_{1/2} + 33S_{1/2} \tag{4}$$

In this case the excitation of the Rydberg level was done with a pulsed dye laser resonant to the $5P_{3/2} \rightarrow 32P_{3/2}$ transition in the presence of a DC electric field. Note that in the excitation scheme transitions to nP states are actually dipole forbidden and are only possible (with limited excitation rates) while deliberately applying electric fields. The $33S_{1/2}$ population, produced by collisions between the atoms in the $32P_{3/2}$ state, was detected through the field-ramp ionization technique 5 µs after the excitation. More details about our experimental setup and detection technique are described in [27]. In Fig. 9(a), the $33S_{1/2}$ population is shown as a function of the DC electric field. Three resonances are distinguishable corresponding to different combinations of the initial states $32P_{3/2,|m|=3/2}$ and $32P_{3/2,|m|=1/2}$ which cannot be resolved by the pulsed laser. The position of the peaks differ from the calculated values by 0.4 V/cm, which we attribute to residual stray electric fields.

We have studied the $33S_{1/2}$ population as a function of time between excitation and detection, which is shown in Fig. 9(b) for an electric field of 10.4 V/cm. Over the first 20 µs population in the $33S_{1/2}$ state builds up, until decay of this state by spontaneous emission results in an exponential decay of the population. The question arises, how the population from $32P_{3/2}$ is transferred into the $33S_{1/2}$ state. In one possible scenario, the dynamics is explained based on a frozen gas picture with many-body diffusion of excitation [10, 11]. Alternatively, the buildup of population may also be explained in a picture where center-of-mass motion of the Rydberg atoms takes place due to large internuclear forces resulting in state-changing collisions [27]. Evidence of such interaction-induced motion was recently pointed out by Li et al. [23].

We are currently conducting experiments to disentangle motionally induced population transfer from Förster resonant energy transfer, as any motion due to interatomic interactions will play an important role for future application of cold Rydberg atoms in the field of quantum computation as has already been pointed out in Sect 3.The same holds for a dephasing of the resonant energy transfer which has been seen by Anderson et al. [28]. In a recent series of experiments we have investigated how the dynamics of resonant

 © 2006 WILEY-VCH Verlag GmbH & Co. KGaA, Weinheim

energy transfer processes depends on the Rydberg density and found good agreement with a Monte-Carlo model describing the coherent evolution of many-body systems [29]. So, while Förster resonances promise large control over the interaction strength they come along with a number of important effects that need further investigation.

6 Conclusion

Quantum information processing in Rydberg systems relies on the strong interaction between Rydberg atoms to realize fast quantum gates. One favorable approach uses this interaction also for an excitation blockade, i.e. a suppression of excitation due to strong (long-range) interactions. Three approaches to control the interaction and produce an excitation blockade have been described and their advantages and disadvantages have been discussed with regard to experimental results.

Induced dipole (van der Waals) interactions appear to be a possible candidate for the blockade effect and a suppression of excitation has already been observed. The vdW interaction is a very weak interaction, but due to its n^{11} scaling reasonable interaction strengths can be reached for high principal quantum numbers. However, the need for high-n states also causes an important drawback of this method. The excitation rate, scaling as n^{-3}, becomes very low, and thus long excitation times are necessary. Dynamic processes, such as acceleration of Rydberg atoms and ionization, can then take place during the excitation, which influences the atomic interactions and the blockade behaviour.

Using Rydberg states with *permanent dipole moments* represents a possible alternative requiring excitation in an electric field. Interaction energies of several MHz at a distance of a few microns can be achieved at small electric fields. This method is limited by the fact that large dipole moments are found only in combination with small excitation rates. Therefore, samples of higher ground state atom density have to be achieved, *e.g.* by magnetic trapping in combination with evaporative cooling, in order to overcome the limitations of the small excitation rate.

The third method is based on *Förster resonances* (resonant energy transfer collisions) to turn a strong dipole-dipole interaction on and off by switching (small) electric fields. This controllable interaction seems to be the most promising approach for the implementation of quantum information processing with Rydberg atoms due to the resonant character of the interaction process. High densities can be achieved by using states with a dipole-allowed excitation (*e.g.* D states). Different effects caused by Förster resonances, such as diffusion of excitation, dephasing of the resonant energy transfer, and interaction-induced motion have already been studied with broadband excitation schemes [10, 11, 27, 28]. We will investigate these resonances and their applicability to quantum information in more detail. The high spectral resolution of our Rydberg excitation scheme will allow for a detailed spectroscopic analysis and for the selective excitation of interacting pairs.

We will further study the autoionization of Rydberg gases mentioned in section 3, since the presence of ions influences the interaction potentials and the behavior of the system strongly. A detailed understanding of the processes leading to ionization is important in order to control Rydberg interactions. Demonstrating the dipole blockade is only the first step towards quantum information processing with Rydberg atoms. As quantum information relies on the coherent superposition of atomic states one has to demonstrate the coherent excitation into Rydberg states as a precursor step to encode qubits. We present investigations of rapid adiabatic passage and coherent two-photon excitation to Rydberg states in another work [30]. In order to observe Rabi oscillations in Rydberg excitation we are currently setting up dedicated optical beam shaping systems for the coherent excitation of Rydberg states and for spatially structuring mesoscopic Rydberg ensembles.

Acknowledgements The project is supported in part by the Landesstiftung Baden-Württemberg in the framework of the "Quantum Information Processing" program, and a grant from the Ministry of Science, Research and Arts of Baden-Württemberg (Az: 24-7532.23-11-11/1). Exchange with the University of São Paulo is financed by the bilateral

© 2006 WILEY-VCH Verlag GmbH & Co. KGaA, Weinheim

PROBRAL program of DAAD and CAPES. We thank G. Raithel, R. Côté, P. Gould and E. Eyler for many valuable discussions and suggestions.

References

[1] D. Bouwmeester, A. Ekert, and A. Zeilinger (eds.), The physics of quantum information (Springer-Verlag, Berlin, 2000).
[2] M. A. Nielsen and I. L. Chuang, Quantum computation and quantum information (Cambridge University Press, Cambridge, 2000).
[3] P. Treutlein, P. Hommelhoff, T. Steinmetz, T. W. Hänsch, and J. Reichel, Phys. Rev. Lett. **92**, 203005 (2004).
[4] D. Schrader, I. Dotsenko, M. Khudaverdyan, Y. Miroshnychenko, A. Rauschenbeutel, and D. Meschede, Phys. Rev. Lett. **93**, 150501 (2004).
[5] T. Calarco, H.-J. Briegel, D. Jaksch, J. I. Cirac, and P. Zoller, J. Mod. Opt. **2137**, 415 (2000).
[6] D. Jaksch, H.-J. Briegel, J. I. Cirac, C. W. Gardiner, and P. Zoller, Phys. Rev. Lett. **82**, 1975 (1999).
[7] M. D. Lukin and P. R. Hemmer, Phys. Rev. Lett. **84**, 2818 (2000).
[8] D. Jaksch, J. I. Cirac, P. Zoller, S. L. Rolston, R. Côté, and M. D. Lukin, Phys. Rev. Lett. **85**, 2208 (2000).
[9] M. D. Lukin, M. Fleischhauer, R. Côté, L. M. Duan, D. Jaksch, J. I. Cirac, and P. Zoller, Phys. Rev. Lett. **87**, 037901 (2001).
[10] W. R. Anderson, J. R. Veale, and T. F. Gallagher, Phys. Rev. Lett. **80**, 249 (1998).
[11] I. Mourachko, D. Comparat, F. de Tomasi, A. Fioretti, P. Nosbaum, V. M. Akulin, and P. Pillet, Phys. Rev. Lett. **80**, 253 (1998).
[12] M. P. Robinson, R. L. Tolra, M. W. Noel, T. F. Gallagher, and P. Pillet, Phys. Rev. Lett. **85**, 4466 (2000).
[13] S. K. Dutta, D. Feldbaum, A. Walz-Flannigan, J. R. Guest, and G. Raithel, Phys. Rev. Lett. **86**, 3993 (2001).
[14] K. Singer, M. Reetz-Lamour, T. Amthor, S. Fölling, M. Tscherneck, and M. Weidemüller, J. Phys. B: At. Mol. Opt. Phys. **38**, 321 (2005).
[15] A. J. Kerman, V. Vuletić, C. Chin, and S. Chu, Phys. Rev. Lett. **84**, 439 (2000).
[16] M. Weidemüller, M. Reetz-Lamour, T. Amthor, J. Deiglmayr, and K. Singer, Laser Spectroscopy XVII, edited by E. A. Hinds, A. Ferguson, and E. Riis (World Scientific, New Jersey, 2005), p. 264.
[17] C. Boisseau, I. Simbotin, and R. Côté, Phys. Rev. Lett. **88**, 133004 (2002).
[18] K. Singer, J. Stanojevic, M. Weidemüller, and R. Côté, J. Phys. B: At. Mol. Opt. Phys. **38**, S295 (2005).
[19] D. Tong, S. M. Farooqi, J. Stanojevic, S. Krishnan, Y. P. Zhang, R. Côté, E. E. Eyler, and P. L. Gould, Phys. Rev. Lett. **93**, 063001 (2004).
[20] K. Singer, M. Reetz-Lamour, T. Amthor, L. G. Marcassa, and M. Weidemüller, Phys. Rev. Lett. **93**, 163001 (2004).
[21] T. F. Gallagher, P. Pillet, M. P. Robinson, B. Laburthe-Tolra, and M. W. Noel, J. Opt. Soc. Am. B **20**, 1091 (2003).
[22] T. F. Gallagher, Rydberg atoms (Cambridge University Press, Cambridge, 1994).
[23] W. Li, P. J. Tanner, and T. F. Gallagher, Phys. Rev. Lett. **94**, 173001 (2005).
[24] M. L. Zimmerman, M. G. Littman, M. M. Kash, and D. Kleppner, Phys. Rev. A **20**, 2251 (1979).
[25] K. A. Safinya, J. F. Delpech, F. Gounand, W. Sandner, and T. F. Gallagher, Phys. Rev. Lett. **47**, 405 (1981).
[26] T. G. Walker and M. Saffman, J. Phys. B **38**, S309 (2005).
[27] A. L. De Oliveira, M. W. Mancini, V. S. Bagnato, and L.G. Marcassa, Phys. Rev. Lett. **90**, 143002 (2003).
[28] W. R. Anderson, M. P. Robinson, J. D. D. Martin, and T.F. Gallagher, Phys. Rev. A **65**, 063404 (2002).
[29] S. Westermann, T. Amthor, A. L. de Oliveira, J. Deiglmayr, M. Reetz-Lamour, and M. Weidemüller, EPJ D (in press) (2006).
[30] J. Deiglmayr, M. Reetz-Lamour, T. Amthor, S. Westermann, A. L. de Oliveira, and M. Weidemüller, Opt. Commun. (in press) (2006).

 © 2006 WILEY-VCH Verlag GmbH & Co. KGaA, Weinheim